Question of hierarchy: Matter effects with atmospheric neutrinos and antineutrinos

D. Indumathi and M. V. N. Murthy

The Institute of Mathematical Sciences, Chennai 600 113, India.

(Received 6 August 2004; published 3 January 2005)

It is by now established that neutrinos mix, have (different) nonzero masses, and therefore oscillate. The oscillation parameters themselves, however, are not all well-known. An open problem is that of the neutrino mass hierarchy. We study the possibility of determining the neutrino mass hierarchy with atmospheric neutrinos using an iron calorimeter detector capable of charge identification such as the proposed MONOLITH and ICAL/INO detectors. We find that such detectors are sensitive to the sign of the mass-squared difference, $\delta_{32} = m_3^2 - m_2^2$, provided the as-yet unknown mixing angle between the first and third generations, θ_{13}, is greater than 6° ($\sin^2 2\theta_{13} > 0.04$). A result with a significance greater than 90% CL requires large exposures (more than 500 kton-years) as well as good energy and angular resolution of the detected muons (better than 15%), especially for small θ_{13}. Hence obtaining definitive results with such a detector is difficult, unless θ_{13} turns out to be large. In contrast, such detectors can establish a clear oscillation pattern in atmospheric neutrinos in about 150 kton-years, therefore determining the absolute value of δ_{32} and $\sin^2 2\theta_{23}$ to within 10%.

DOI: 10.1103/PhysRevD.71.013001 PACS numbers: 14.60.Pq

I. INTRODUCTION

Recent experimental results from the observations of solar, atmospheric and reactor neutrinos have provided compelling evidence for neutrino oscillations [1–3]. Until recently the evidence for neutrino oscillation was indirect, with a small window still available for other possibilities such as neutrino decay. The latest results from the Super-Kamiokande (Super-K) collaboration [4], presenting the evidence for an ''oscillation minimum'' in the observation of atmospheric neutrinos, seem to provide for the first time clear and unambiguous evidence for the oscillation hypothesis [5,6] and hence of nonzero (and different) neutrino masses and mixing. Recently, data is also available from the long-baseline experiment K2K [7].

Clearly the focus from now on will be to determine precisely the mixing parameters and mass-squared differences apart from the observation of the oscillation pattern beyond the first minimum. An important question that still remains open is the hierarchy of the masses. Within the three neutrino mixing framework, the results on solar neutrinos prefer the dominant mass eigenstates in ν_e to have the hierarchy $m_2 > m_1$ so that the mass-squared difference[1] $\delta_{21} = m_2^2 - m_1^2 > 0$. The sign of the other mass-squared difference δ_{32} (equivalently δ_{31} since it is so much larger than δ_{21}) is not known.

The issue of the neutrino mass hierarchy (and measurement of the (13) mixing angle) was discussed by Tabarelli de Fatis [8] through a measurement of muon neutrino and antineutrino events in a magnetised iron calorimeter. In a recent analysis, Palomares-Ruiz and Petcov [9] have discussed the resolution of the issue of hierarchy of neutrino masses in magnetised iron calorimeters by looking at the ratio (and difference) of events with μ^+ and μ^- due to atmospheric muon neutrino and antineutrino interactions.

In principle an iron calorimeter (ICAL) detector with charge identification capability as has been proposed by the MONOLITH [10], MINOS [11] and ICAL/INO [12] collaborations can resolve this issue; the question at hand is one of feasibility and exposure times.

In this paper we focus on a new *difference asymmetry* that is especially suited to probe the mass hierarchy. This asymmetry is constructed from observables involving the detection of muon neutrinos (and antineutrinos) through charged current interactions with muons in the final state. Palomares-Ruiz and Petcov showed that the direct and inverted hierarchies could be discriminated by studying the *magnitude* of certain asymmetries; in contrast, the new asymmetry probes the hierarchy issue via its *sign*, which is surely a more robust signature. Provided $\sin^2 2\theta_{13} > 0.04$, an ICAL detector is sensitive to the mass hierarchy. A result with a significance greater than 90% CL requires large exposures of more than 500 kton-years as well as good energy and angular resolution of the detected muons (better than 15%), especially for small θ_{13}. Hence obtaining definitive results with such a detector is difficult, unless θ_{13} turns out to be large.

Furthermore, such an asymmetry is not as sensitive to the magnitude of θ_{13}; in the case of a positive result it may only place a lower bound on this parameter. The issue of θ_{13} therefore may not be resolved in such detectors using atmospheric neutrinos alone.

In Sec. II we present some details of the oscillation probabilities and their dependence on masses and mixing parameters after summarizing the status of their determination within the three neutrino framework. Some features of these probabilities within some reasonable approximation such as single-scale dominance are presented in a

[1]All oscillation experiments are sensitive to mass-squared differences rather than the absolute scale of the masses themselves.

semianalytic treatment. The new asymmetry and its sensitivity to the hierarchy are discussed here as also the crucial question of binning the data to maximize this asymmetry. In Sec. III we analyze the results numerically for the event rates both together and separately for different charged-lepton final states using the NUANCE code [13] for atmospheric neutrinos distributed according to the 3-D Honda flux [14]. We discuss the sensitivity of the ICAL detector to the hierarchy of neutrino masses. This obviously depends on the mixing parameters. We highlight the sensitivity to the two unknown parameters, the (13) mixing angle and the sign of δ_{32}. In Sec. IV we generate events using the NUANCE neutrino generator and study the impact of statistical errors and fluctuations on the rates and asymmetries. The effect of detector resolution and cuts on the observables is also discussed. In Sec. V we present our conclusions.

II. THREE-FLAVOR OSCILLATIONS

An understanding of the gamut of data from solar, atmospheric and reactor neutrinos requires a mixing scheme with at least three neutrinos in which the neutrino flavor states $|\nu_\alpha\rangle$, $(\alpha = e, \mu, \tau)$ are linear superpositions of the neutrino mass eigenstates $|\nu_i\rangle$, $(i = 1, 2, 3)$, with masses m_i :

$$|\nu_\alpha\rangle = \sum_i U_{\alpha i}|\nu_i\rangle. \tag{1}$$

Here U is the 3×3 unitary matrix which may be parametrized as [6] (ignoring Majorana phases):

$$U = \begin{pmatrix} c_{12}c_{13} & s_{12}c_{13} & s_{13}e^{-i\delta} \\ -c_{23}s_{12} - s_{23}s_{13}c_{12}e^{i\delta} & c_{23}c_{12} - s_{23}s_{13}s_{12}e^{i\delta} & s_{23}c_{13} \\ s_{23}s_{12} - c_{23}s_{13}c_{12}e^{i\delta} & -s_{23}c_{12} - c_{23}s_{13}s_{12}e^{i\delta} & c_{23}c_{13} \end{pmatrix}. \tag{2}$$

Here $c_{12} = \cos\theta_{12}$, $s_{12} = \sin\theta_{12}$ etc., and δ denotes the CP violating (Dirac) phase. By definition, the 3×3 neutrino mass matrix M_ν is diagonalized in the charged-lepton mass basis by U:

$$U^\dagger M_\nu U = \mathrm{diag}(m_1, m_2, m_3). \tag{3}$$

The parameters involved are the mixing angles θ_{ij} and the mass-squared differences $\delta_{ij} \equiv m_i^2 - m_j^2$. A combined analysis [15] of the data from all the experiments gives the following best fits to the oscillation parameters:

(i) A combination of solar neutrino experiments and the KamLAND reactor experiment gives

$$5.4 \times 10^{-5}\mathrm{eV}^2 < \delta_{21} < 9.4 \times 10^{-5}\mathrm{eV}^2, \qquad 0.30 < \tan^2\theta_{12} < 0.64, \tag{4}$$

with the best-fit values given by $\delta_{21} = 6.9 \times 10^{-5}\mathrm{eV}^2$ and $\tan^2\theta_{12} = 0.40$. Note, in particular, that $m_2^2 > m_1^2$.

(ii) A combination of atmospheric neutrino experiments and the K2K experiment gives

$$1.4 \times 10^{-3}\mathrm{eV}^2 < |\delta_{32}| < 5.1 \times 10^{-3}\mathrm{eV}^2, \qquad \sin^2 2\theta_{23} > 0.86, \tag{5}$$

with the best-fit values given by $|\delta_{32}| = 2.0 \times 10^{-3}\mathrm{eV}^2$ and $\sin^2 2\theta_{23} = 1$. Note that there is as-yet no determination of the sign of this mass-squared difference.

(iii) The CHOOZ bound on the effective mixing angle using the above parametrization is,

$$\sin^2 2\theta_{13} < 0.249 \qquad (99.73\%\mathrm{C.L.}) \tag{6}$$

so that $\theta_{13} < 14.9°$.

Inclusion of matter effects on the neutrino oscillation probabilities has a complicated dependence on these parameters; furthermore, the oscillation probability can only be computed numerically using a reference model for the variation of earth's density. Before we present the exact numerical results, we first discuss a simplified analytical model in vacuum and matter.

A. Probabilities in Vacuum

In order to focus on the issues involved and their disentanglement we first discuss the vacuum oscillations (actually the muon neutrino survival) probabilities. The survival probability of a muon neutrino of energy E (in GeV) after traversing a distance L (in km) is given by

$$P_{\mu\mu} = 1 - [2U_{\mu 1}U_{\mu 2}]^2\sin^2\left(\frac{1.27\delta_{21}L}{E}\right) - [2U_{\mu 2}U_{\mu 3}]^2\sin^2\left(\frac{1.27\delta_{32}L}{E}\right) - [2U_{\mu 1}U_{\mu 3}]^2\sin^2\left(\frac{1.27\delta_{31}L}{E}\right), \tag{7}$$

where we have neglected the CP violating phase. Note that in vacuum the probabilities are the same for both neutrinos and antineutrinos. In Fig. 1 we plot the survival probability of ν_μ as a function of L/E for $\delta_{32} = 2 \times 10^{-3}$ eV^2 and $\theta_{13} = 9°$, with other parameters fixed to their best-fit values. For comparison we have also shown the two-generation oscillation probability,

$$P^{(2)}_{\mu\mu} = 1 - \sin^2 2\theta_{23}\sin^2\left(\frac{1.27\delta_{32}L}{E}\right), \tag{8}$$

which has been widely used to fit $|\delta_{32}|$ and $\sin\theta_{23}$ from data.

Notice that the three generation formula reduces to the two-generation one only after setting $\theta_{13} = 0$ and $\delta_{21} = 0$. Even though there are two oscillating terms (frequencies)

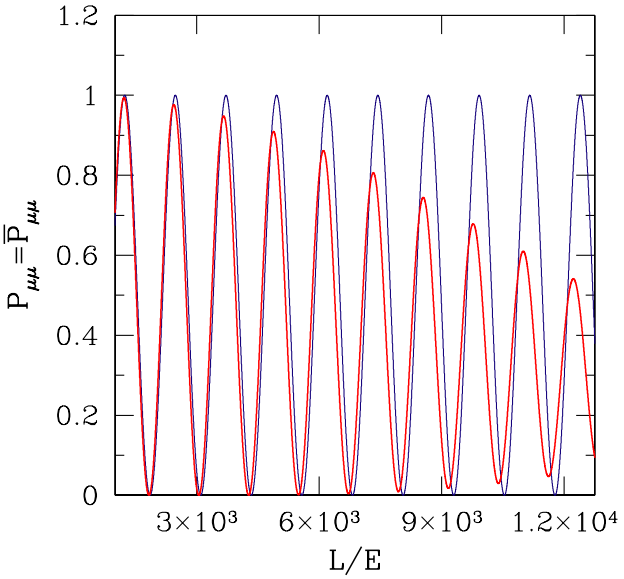

FIG. 1 (color online). Survival probability of muon-neutrinos in vacuum with two and three neutrino mixing scenarios. We have used $|\delta_{32}| = 2 \times 10^{-3}$, $\theta_{23} = \pi/4$ in both. For the three generation probability we have used in addition $\theta_{13} = 9^o$ and the best-fit values of other parameters as given in the text.

controlling the survival probability, the value of the probability at small L/E is dominated by the last two terms in Eq. (7). In turn, this implies that the first observable probability minimum is roughly independent of both δ_{21} and θ_{13}, even for θ_{13} as large as the CHOOZ limit. At larger values of L/E, when $\delta_{21}L/E$ becomes large, the subdominant frequency controlled by δ_{21} has substantial effect.

This can be seen from Fig. 1 where both the two-flavor and three-flavor probabilities are plotted as a function of L/E. In fact, for very large L/E, and for this typical set of oscillation parameters, the vacuum probability $P_{\mu\mu}$ averages to $\approx 3/8$ and not to $1/2$ as is the case for two-generation mixing.

Notice that the probabilities in vacuum are the same for both neutrinos and antineutrinos and depend only on the absolute value of the mass-squared differences. However, the inclusion of three flavors automatically turns on matter effects which alter these vacuum results; we now examine the modification of these expressions due to matter effects.

B. Probabilities in matter

In order to simplify the analysis, we first consider the propagation of neutrinos and antineutrinos produced in the atmosphere in a slab of constant-density ρ (in gms/cc)[16]. In this case, we can retain the same expressions as in vacuum for the probabilities, see Eq. (7), but replace the mass-squared differences and mixing angles by the corresponding matter-modified effective values obtained by diagonalizing the matter-dependent matrix (Hamiltonian):

$$U\begin{pmatrix} 0 & 0 & 0 \\ 0 & \delta_{21} & 0 \\ 0 & 0 & \delta_{31} \end{pmatrix}U^\dagger + \begin{pmatrix} A & 0 & 0 \\ 0 & 0 & 0 \\ 0 & 0 & 0 \end{pmatrix}, \tag{9}$$

where

$$A = 2\sqrt{2}G_F n_e E = 7.63 \times 10^{-5}\ \text{eV}^2 \rho(\text{gm/cc}) E(\text{GeV})\text{eV}^2. \tag{10}$$

Here G_F and n_e are the Fermi constant and electron number density in matter and ρ is the matter density. Further simplification arises because $\delta_{21} \ll |\delta_{31}|$ and we can treat the propagation in matter as a one mass-scale problem involving only $|\delta_{32}| \approx |\delta_{31}|$. The matter dependent mixing angle $\theta_{12,m}$ may be approximately written as

$$\sin 2\theta_{12,m} \approx \frac{\sin 2\theta_{12}}{\sqrt{[\cos 2\theta_{12} - (A/\delta_{21})\cos^2\theta_{13}]^2 + \sin^2 2\theta_{12}}}. \tag{11}$$

The condition for ''resonance'' in the (12) channel is given by $\delta_{21}\cos 2\theta_{12} = A\cos^2\theta_{13}$ which roughly translates to the condition, $\rho E \approx 0.5$. We note in passing that the resonance in the (12) sector for atmospheric neutrinos has a very different character from its solar counterpart. For example, for energies above 1 GeV, the resonance occurs at extremely small densities, even in the atmosphere itself for some energies! Furthermore, the resonance width which is determined by $\sin 2\theta_{12}$ is rather broad, with the tail extending below $A = 0$ so that the effect of matter in this sector on both neutrinos and antineutrinos will be roughly similar.

This also implies that $\sin 2\theta_{12,m}$ is rather small for neutrinos or antineutrinos of few GeV energy even in low density regions such as the earth's mantle—in fact at high densities and energies, we have

$$\sin 2\theta_{12,m} \approx \frac{\sin 2\theta_{12}}{\rho E}, \tag{12}$$

so that one can neglect the term depending on δ_{21} for multi-GeV atmospheric neutrino propagation in earth matter. Indeed the same argument also holds for antineutrinos since the equation above[2] holds for them as well.

The effect of matter on the angle θ_{13} is nontrivial and is given by

$$\sin 2\theta_{13,m} = \frac{\sin 2\theta_{13}}{\sqrt{[\cos 2\theta_{13} - (A/\delta_{32})]^2 + (\sin 2\theta_{13})^2}}. \tag{13}$$

The resonance condition in the (13) channel is then given by $\delta_{32}\cos 2\theta_{13} = A$ with a width $\delta A = \delta_{32}\sin 2\theta_{13}$. Since $\sin^2 2\theta_{13}$ is small, the resonance is rather sharp. This con-

[2]This term in the matter-dependent analogue of Eq. (7) is often neglected citing the reason that $\delta_{21}/\delta_{31} \ll 1$. Actually, $\delta_{21}L/E$ can be of the order of unity for atmospheric neutrinos; it is the smallness of the *coefficient* of this term that allows it to be dropped.

dition is satisfied for range of values $13 < \rho E < 40$ for $1 < \delta_{31}/10^{-3} < 3$ eV^2. The average mantle density is about 4–5 gm/cc and the resonance occurs for energies greater than 4 GeV. In the core, where the density exceeds nine gm/cc the resonance condition is satisfied with even smaller energy. For antineutrinos the matter effects come with opposite sign, $A \to -A$, so that resonance occurs with the inverted mass hierarchy $\delta_{31} < 0$.

The main observable effect due to propagation in matter comes from the matter-dependent angle $\theta_{13,m}$ since for all practical purposes we can set

$$\sin 2\theta_{23,m} \approx \sin 2\theta_{23}. \tag{14}$$

The approximate survival probability[16] for ν_μ can be written as

$$\begin{aligned} P^m_{\mu\mu}(A, \delta_{32}) \approx 1 &- \sin^2 2\theta_{23}[\sin^2\theta_{13,m}\sin^2\Delta^m_{21} \\ &+ \cos^2\theta_{13,m}\sin^2\Delta^m_{32}] \\ &- \sin^2 2\theta_{13,m}\sin^4\theta_{23}\sin^2\Delta^m_{31}, \end{aligned} \tag{15}$$

where

$$\begin{aligned} \Delta^m_{21} &= \frac{1.27\delta_{32}L}{E}\,\frac{1}{2}\left[\frac{\sin 2\theta_{13}}{\sin 2\theta_{13,m}} - 1 - \frac{A}{\delta_{32}}\right], \\ \Delta^m_{32} &= \frac{1.27\delta_{32}L}{E}\,\frac{1}{2}\left[\frac{\sin 2\theta_{13}}{\sin 2\theta_{13,m}} + 1 + \frac{A}{\delta_{32}}\right], \\ \Delta^m_{31} &= \frac{1.27\delta_{32}L}{E}\left[\frac{\sin 2\theta_{13}}{\sin 2\theta_{13,m}}\right]. \end{aligned} \tag{16}$$

Note that for sufficiently large values of A/δ_{32}, all the three scales are of the same order of magnitude including Δ^m_{21} which cannot therefore be neglected.

If we further take $\sin^2\theta_{13}$ to be small, which it is, and restrict the analysis to values of A away from resonance, then we can expand the ratio

$$\frac{\delta \sin 2\theta_{13}}{\sin 2\theta_{13,m}} \approx (\delta - A) + \frac{2A\delta}{\delta - A}\sin^2\theta_{13}, \tag{17}$$

where we have used the notation $\delta \equiv \delta_{32}$. As a result the survival probabilities for ν_μ and $\bar{\nu}_\mu$ can be simplified further and written, to order $\sin^2\theta_{13}$, as,

$$\begin{aligned} P^m_{\mu\mu}(A, \delta) \approx P^{(2)}_{\mu\mu} &- \sin^2\theta_{13}\left[\frac{A}{\delta - A}T_1 + \left(\frac{\delta}{\delta - A}\right)^2\right. \\ &\left.\times (T_2\sin^2[(\delta - A)x] + T_3)\right], \end{aligned} \tag{18}$$

$$\begin{aligned} \overline{P}^m_{\mu\mu}(A, \delta) \approx P^{(2)}_{\mu\mu} &- \sin^2\theta_{13}\left[-\frac{A}{\delta + A}T_1 + \left(\frac{\delta}{\delta + A}\right)^2\right. \\ &\left.\times (T_2\sin^2[(\delta + A)x] + T_3)\right], \end{aligned}$$

where $x \equiv 1.27L/E$. Here $P^{(2)}_{\mu\mu} = 1 - \sin^2 2\theta_{23}\sin^2(x\delta)$ is the 2-generation muon neutrino survival probability that is independent of matter effects as well as $\sin^2\theta_{13}$. The matter dependence appears in the remaining terms, where

$$\begin{aligned} T_1 &= x\delta\sin^2 2\theta_{23}\sin 2\delta x, \\ T_2 &= 4\sin^4\theta_{23}, \\ T_3 &= \sin^2 2\theta_{23}(\sin^2 Ax - \sin^2\delta x). \end{aligned}$$

Notice that the survival probability for the antineutrinos, $\overline{P}^m_{\mu\mu}$, is given by the replacement $A \to -A$ in $P^m_{\mu\mu}$. Both probabilities are invariant under $(A, \delta) \leftrightarrow (-A, -\delta)$.

Several important points emerge from this analysis:

(i) As was noticed in the analysis of the vacuum probabilities with three flavors, there are two mass scales and their associated frequencies. Even though one of the scales is small in magnitude, $\delta_{21} \ll \delta_{31}$, it does make an impact on the survival probability due to the large L/E available; this happens because a large range of L/E is available for atmospheric neutrinos. This makes the 3-flavor results differ strongly from the 2-flavor ones in the large L/E region, in the vacuum case.

(ii) The matter effect, however, effectively removes one of these frequencies controlled by δ_{21} such that the oscillations are controlled by the frequency determined by δ_{32} and to a lesser extent by the matter term A. In other words, the deviation of the 3-flavor probability from the 2-flavor one at large L/E disappears when matter effects are turned on. The residual matter effect in atmospheric neutrinos is thus a subleading effect.

(iii) Thus the matter dependent $P^m_{\mu\mu}$ and $\overline{P}^m_{\mu\mu}$ resemble the two-generation probability curve shown in Fig. 1 rather than the three generation one. In fact the first dip is almost completely unaltered by the matter effects, and the average behavior for large L/E is similar to the two-generation case. This in fact justifies the attempts to get bounds on $|\delta_{32}|$ and $\sin 2\theta_{23}$ using fits to the Super-K data within the two-flavor oscillation formalism.

(iv) Therefore the sensitivity to θ_{13} and the sign of δ_{32} are hidden in the subleading effects which show up in the oscillation frequency, the width and the amplitude after the first dip, and are maximal for intermediate values of L/E. The matter effect is more pronounced for (anti-)neutrinos in the case of the (inverted) direct hierarchy, since the amplitude of the matter-dependent term is enhanced (decreased) when δ_{32} and A have the same (opposite) sign, as can be seen from Eq. (18).

All of the above statements apply appropriately (by interchanging the matter effects for neutrinos and antineutrinos) for both the direct and inverted hierarchies. This *exchange symmetry* will however be broken once the cross-sections are taken into account since the neutrino cross-sections are on the average a factor of 2 more than the antineutrino cross-sections. Since matter effects are enhanced for neutrinos in the case of the direct hierarchy,

such a hierarchy will be more favorable for detection due to the larger events sample for the same exposure time.

III. EVENT RATES AND ASYMMETRIES

The arguments of the previous section clearly indicate that the main effect of matter on the survival probability is to reduce it to a single frequency (which, however, is not a constant since it depends both on energy and the density) oscillation, whereas in vacuum there are clearly two well-separated oscillations.

The inclusion of matter effects through a 3-flavor analysis is complicated by an additional energy dependence. While the survival probability in the 2-flavor case depends only on the ratio $x = L/E$, that in 3-flavors depends explicitly on both x and E, the latter through the matter term. The experimental observable is the event rate in the detector. The fully differential event rate for neutrinos of flavor α to be detected is given by the general expression:

$$\frac{\mathrm{d}^2 N^\alpha}{\mathrm{d}\ln E \mathrm{d}x} = K_y \sum_\beta P_{\beta\alpha}(E, x)\Phi_\beta(E, x)\sigma_\alpha(E), \qquad (19)$$

where $x = L/E$ and σ_α is the total interaction cross-section for the α type neutrino to interact with the detector material. Here $P_{\beta\alpha}$ is the conversion probability of a neutrino of flavor β to a flavor α.

The flux-dependent term $\Phi_\alpha(E, x)$ is obtained from the doubly-differential neutrino (or antineutrino) flux of flavor α, $\mathrm{d}^2\phi_\alpha(E, z)/\mathrm{d}\ln E \mathrm{d}z$, which is a function of the energy E and zenith (actually nadir) angle $z = \cos\theta$, by multiplying with a suitable Jacobean factor.

The factor K_y is the detector dependent factor measured in units of kton-years. The detector is assumed to be mainly made up of magnetized iron with active detector elements. In the MONOLITH and ICAL/INO proposals, the active detector elements are glass resistive plate gas filled chambers (RPCs). In either of these proposals the detector mass is almost entirely ($> 98\%$) due to its iron content. We will be interested here in *event ratios*; hence the factor K_y and other actual detector details are not necessary for the analysis in this section. However, we assume that the detector is capable of identifying the charge of the muons in the final state with good precision.

The distance of propagation L of the neutrino from the point of production to the detector is obtained from

$$L = \sqrt{(R + L_0)^2 - (R\sin\theta)^2} - R\cos\theta, \qquad (20)$$

where $\theta = 0$ corresponds to neutrinos reaching the detector vertically downwards after a distance L_0 which is the average height above the surface of the earth at which the atmospheric neutrinos are produced. We take this to be about 15 kms, as is the convention. Here R is the radius of the earth.

The event rate in a given bin of $x = L/E$ is,

$$N^\alpha_{\mathrm{bin}}(x) = \int_{\mathrm{bin}} \mathrm{d}x \int_{E_{\mathrm{min}}} \frac{\mathrm{d}^2 N^\alpha}{\mathrm{d}\ln E \mathrm{d}x}; \qquad (21)$$

henceforth we discuss only the case of muon-neutrinos, $\alpha = \mu$. For the case of atmospheric neutrinos of interest here, both $P_{e\mu}$ and $P_{\mu\mu}$ contribute in the expression above. However, due to the smallness of the (13) mixing angle, θ_{13}, the contribution of $P_{e\mu}$ is very small and is maximum near large L/E where it is about 10–20% (5%) for neutrinos (antineutrinos).

The event rate is expressed as a function of x, averaged over a bin-width that will be appropriately chosen to maximise the sensitivity to the sign of δ_{32}. The expression given in Eq. (21) is the best-case scenario since the integration is over the neutrino or antineutrino energy. We discuss the effect of including the detector resolution functions in the next section.

In order to proceed further we also distinguish between the up-coming and down-going neutrinos (and antineutrinos). It is obvious that the down-going particles travel a much smaller path-length of $15 < L < 400$ km in matter. Hence effects of oscillation are expected to be negligible for these neutrinos[3].

A useful measure of oscillations is the ratio of up-coming to down-going neutrinos with nadir/zenith angles interchanged. This is clear from Fig. 2. The fluxes of atmospheric neutrinos from directions θ and $(\pi - \theta)$ are expected to be similar in the absence of oscillations, especially for larger energies, $E >$ few GeV. Since the path-length traversed, L, is related to θ as

$$L = f(|\cos\theta|) - R\cos\theta,$$

(see Eq. (20)), the replacement $\theta \leftrightarrow (\pi - \theta)$ effectively changes the sign of the second term in the equation above, thus taking, for instance, a down-going neutrino to an up-coming one. The ratio of events in the up-down directions for a given $x = L/E$, therefore, reflects the asymmetry of the up-down fluxes, due to oscillations. We define [17]

$$\mathcal{R} = \frac{U}{D}(x) = \frac{\text{No.of events from up-coming muon neutrinos}(x)}{\text{No.of events from down-going muon neutrinos}(\tilde{x})},$$

where $\tilde{x} = x[\theta \leftrightarrow (\pi - \theta)]$ and the number of up-coming (U) or down-going (D) events is calculated using Eq. (21). Similarly $\overline{U}/\overline{D}$ defines the corresponding up-down ratio for antineutrinos. Since the effect of oscillations on the denominator is small, the ratio $\mathcal{R}$ is effectively the ratio of oscillated to unoscillated events with the same L/E.

[3]This is not true for very horizontal neutrinos; however, if the detector geometry consists of horizontally stacked iron-plates, such very horizontal events cannot be observed.

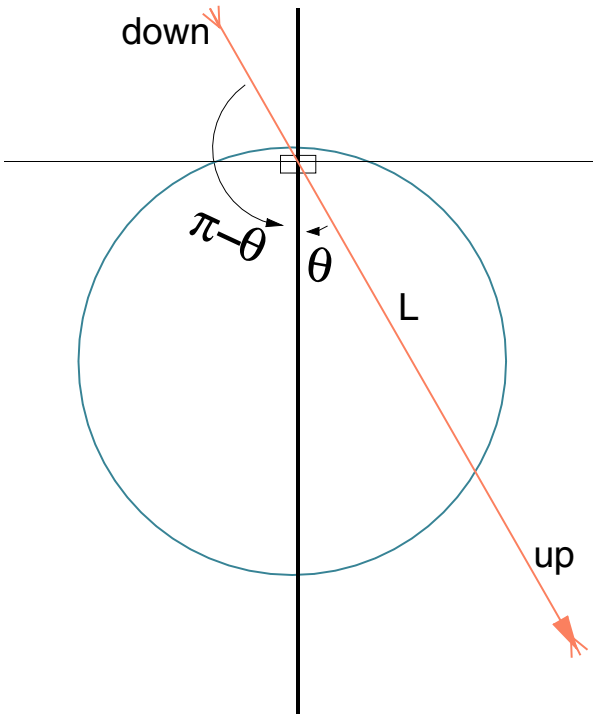

FIG. 2 (color online). A schematic of the relation between upcoming and down-going neutrinos with $\theta \leftrightarrow (\pi - \theta)$.

Thus, while reflecting the effect of oscillations, this ratio also minimizes errors due to the uncertainties in the overall flux normalization (which can be as large as 30%). Such a ratio, and its sensitivity to the parameters of neutrino oscillations, has been well-studied before; in particular, detailed studies have been carried out by the MONOLITH collaboration [10]. We shall not repeat the results of such a study here; however, we will use the information on the absolute value of δ_{32} that such a study will yield in order to analyze matter effects and its implication for the neutrino mass hierarchy.

We now proceed with the numerical details. All calculations presented are done using the NUANCE neutrino generator. The atmospheric neutrino flux given by Honda *et al.* [14] is used. The code generates oscillation probabilities based on the three neutrino oscillation framework of Barger *et al.* [18]. The earth matter effects are calculated using the Preliminary Reference Earth Model (PREM) [19] for the variation in matter density.

Apart from L and E, the probabilities depend on the parameters δ_{21}, δ_{32}, θ_{12}, θ_{23}, and θ_{13} (the CP phase has been set to zero). Since the focus of this paper is the issue of matter effects and mass hierarchy, we fix the other parameters at their best-fit values[4]:

$$\begin{aligned} \delta_{21} &= 7.0 \times 10^{-5}\ \text{eV}^2; \\ \tan^2\theta_{12} &= 0.39; \\ \sin^2 2\theta_{23} &= 1.0, \end{aligned}$$

and vary only the parameters of interest, viz., δ_{32} (both in magnitude and in sign) and θ_{13}. We restrict ourselves to the latest Super-K limits on the magnitude of δ_{32}: $1 \leq |\delta_{32}/10^{-3}| \leq 3\ \text{eV}^2$ and the CHOOZ bound $\sin^2 2\theta_{13} < 0.249$ ($\theta_{13} < 14.9°$).

The NUANCE neutrino generator calculates the probabilities, fluxes and cross-sections suitably in bins of E and $\cos\theta$ for use in generating events. Event rates, as given in Eq. (19), were first computed using these tables, with suitable interpolation and integration over the variables with a cut on the energy, $E_{\text{min}} = 4$ GeV. This cut was optimized to maximize the matter-dependent effects, as we shall see below.

We show the variation of the up/down events ratio $\mathcal{R}$ as a function of L/E for both ν_μ and $\overline{\nu}_\mu$ in Figs. 3 and 4 for direct ($m_3^2 > m_2^2$) and inverted ($m_3^2 < m_2^2$) hierarchies. Results are shown for $|\delta_{32}| = 1, 2, 3 \times 10^{-3}$ eV^2 and for $\theta_{13} = 5°$(Fig. 3) and 11°(Fig. 4) to show the sensitivity to these two parameters.

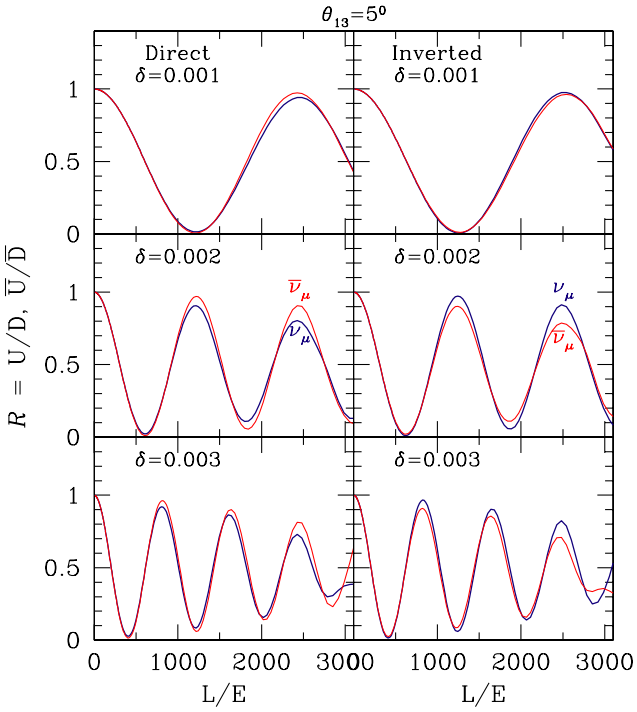

FIG. 3 (color online). Up/down event ratios for ν_μ shown as thick (blue) lines and $\bar{\nu}_\mu$ as thin (red) lines as a function of L/E for $E > 4$ GeV. The three horizontal panels correspond to $\delta \equiv |\delta_{32}| = 1, 2, 3 \times 10^{-3}$ eV^2. The vertical panels correspond to the direct ($\delta_{32} > 0$) and inverted ($\delta_{32} < 0$) hierarchy for $\theta_{13} = 5°$. All other parameters are kept at their best-fit values as given in the text.

[4]These values have altered somewhat with the latest results from Super-K and KamLAND; however, they should not affect our conclusions or even our numerical calculations significantly.

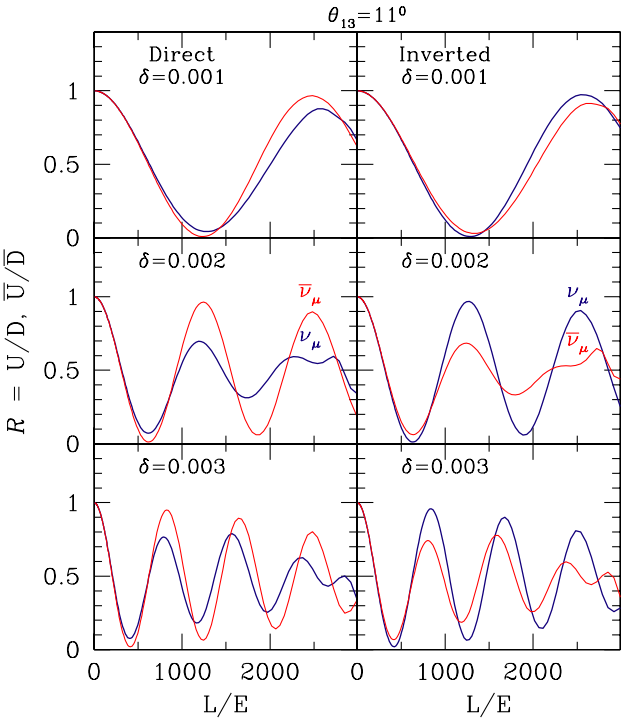

FIG. 4 (color online). Same as in Fig. 3 with $\theta_{13} = 11^o$.

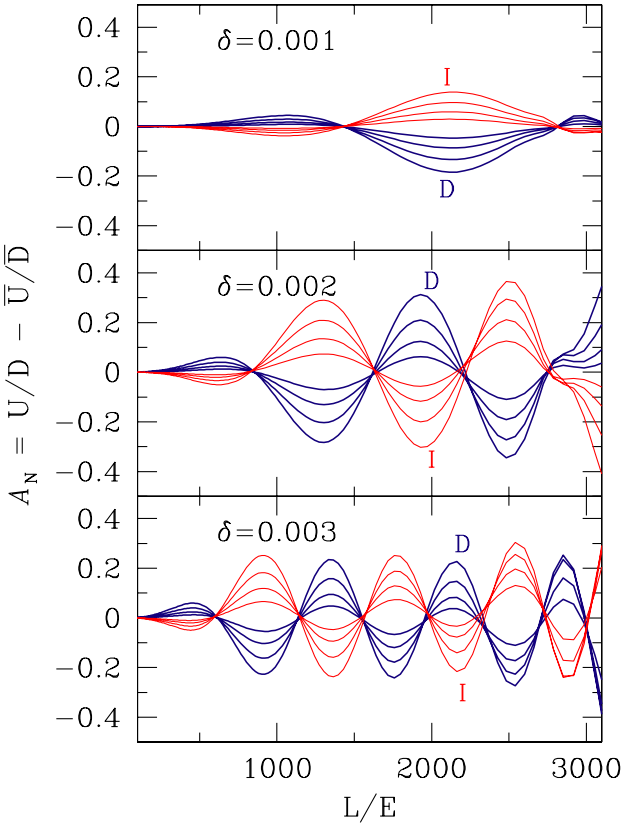

FIG. 5 (color online). The difference asymmetry (difference of up/down ratios of muon-neutrinos and antineutrinos) as a function of L/E for $E > 4$ GeV. The three panels correspond to $\delta \equiv |\delta_{32}| = 1, 2, 3 \times 10^{-3}$ eV^2. The thick (blue) curves correspond to the direct $\delta_{32} > 0$ and the thin (red) curves correspond to the inverse $\delta_{32} < 0$ hierarchy. The innermost curve in each envelope corresponds to $\theta_{13} = 5°$ and the outermost corresponds to $\theta_{13} = 11°$ with $7°$ and $9°$ in-between. The best-fit values of other parameters are given in the text.

It is obvious from Figs. 3 and 4 that there is very little sensitivity to the sign of δ_{32} at small values of θ_{13}. For example, it is clear that atmospheric neutrino experiments can say very little about the hierarchy problem below $\theta_{13} = 6°$ ($\sin^2 2\theta_{13} = 0.04$). However, the sensitivity to the sign increases with the magnitude of θ_{13}.

It is important to note that the position of the first minimum is *independent* of both θ_{13} and the sign of δ_{32} but depends only on the magnitude of the latter. Hence it can be reliably used to determine the magnitude of δ_{32} as a precursor to determining its sign with the same experimental set-up.

It is clear that the neutrino and antineutrino up/down event ratios are different from each other as well as different with direct and inverted mass hierarchies (due to matter effects); the distinction (and hence measurement possibilities) between the two hierarchies can be amplified by defining the asymmetry,

$$\mathcal{A}_N(x) = \frac{U}{D}(x) - \frac{\overline{U}}{\overline{D}}(x). \tag{22}$$

The asymmetry, calculated numerically, and integrated over $E_{\rm min} > 4$ GeV is plotted as a function of L/E in Fig. 5 for $\delta_{32} = 1, 2, 3 \times 10^{-3}$ eV^2. The thick (blue) curves in the figure correspond to the direct mass hierarchy (labeled D) and the thin (red) curves to the inverted mass hierarchy (labeled I). The curves in each envelope correspond to $\theta_{13} = 5, 7, 9, 11$ degrees ($\sin^2 2\theta_{13}$ from 0.03–0.14) with the asymmetry increasing symmetrically with θ_{13} about the $\mathcal{A}_N = 0$ line for direct and inverse hierarchies. It is seen that the direct and inverted asymmetries are exactly out of phase.

The maximum divergence between the direct and inverted hierarchies is smaller in the first envelope than in the second; these correspond to the first dip and rise in the up/down events ratio (equivalently, in $P_{\mu\mu}$). We will see in the next section that the statistically significant region with maximum number of events corresponds to these first few envelopes, i.e., to the range $500 < L/E < 1500$ for all the three values of the δ_{32} considered here.

For neutrinos of energy about 5–7 GeV the interesting region thus corresponds to distances 4000–10000 km with an average around 7000 km [20] which is really the magic baseline where matter effects are largest and the effect of the CP violating phase is negligible (though we have set this phase to zero).

In order to understand why the direct and inverted asymmetries are out of phase, it is convenient to appeal to the analytic expressions for the probabilities discussed in the previous section.

Since the events in a given L/E bin are largely saturated by the smallest allowed energy in that bin (the flux falls faster than $1/E^2$), the effect of the cross-section factor is small and the up/down events ratio is well-approximated by the flux-averaged probability $P^{\rm av}_{\alpha\beta}$ defined below:

$$P^{\rm av}_{\alpha\beta}(\langle x\rangle) = \frac{\int_{\rm bin} {\rm d}x \int_{E_{\rm min}}^{\infty} \frac{{\rm d}E}{E} P_{\alpha\beta}(E,x)\Phi_\alpha(E,x)}{\int_{\rm bin} {\rm d}x \int_{E_{\rm min}}^{\infty} \frac{{\rm d}E}{E} \Phi_\alpha(E,x)}. \qquad (23)$$

Considering only the dominant contribution from $P_{\mu\mu}$ to this expression, we see that $\mathcal{A}_N$ corresponds to the approximate difference asymmetry,

$$\mathcal{A}_N \approx \mathcal{A}(A,\delta_{32}) \equiv P^{\rm av}_{\mu\mu} - \overline{P}^{\rm av}_{\mu\mu}. \qquad (24)$$

Here $\overline{P}$ denotes the survival probability for anti-neutrinos which is obtained from the corresponding neutrino survival probability P by the replacement $A \longrightarrow -A$ and the explicit dependences on the energy and path-length E and L have been suppressed for clarity.

In the single mass-scale dominance approximation (with $\delta_{21} \ll \delta_{31}, A$), the survival probability for neutrinos and anti-neutrinos involves only the ratio A/δ_{32}. As a result we have,

$$\begin{aligned} P^{\rm av}_{\mu\mu}(A,\delta_{32}) &= P^{\rm av}_{\mu\mu}(-A,-\delta_{32}); \\ P^{\rm av}_{\mu\mu}(A,-\delta_{32}) &= P^{\rm av}_{\mu\mu}(-A,\delta_{32}). \end{aligned} \qquad (25)$$

This is easy to see from the approximate expressions for the case of constant-density matter in Eq. (15). It follows therefore, for a given E and L,

$$\mathcal{A}(A,\delta_{32}) = -\mathcal{A}(A,-\delta_{32}), \qquad (26)$$

for constant matter density. Note that the amplitude is not a constant but depends on the energy and distance travelled. In other words, the asymmetry oscillates with L/E while being exactly out of phase for the direct and inverse hierarchies. It appears (as can be seen from Figs. 3 and 4) that this feature survives in the events ratio computed using the exact formula without using the approximation defined in Eq. (24) above.

Note also that the oscillation wavelength is a complicated function of both the matter-dependent terms as well as the mass-squared difference, δ_{32}. However, the matter effect is not so significant in the case of (anti-)neutrinos with (direct) inverted hierarchy, where the oscillation extrema are essentially determined by the matter-independent condition,

$$\frac{1.267|\delta_{32}|L}{E} = n\frac{\pi}{2}.$$

So far, we have discussed the asymmetry where separation of neutrino and antineutrino events is a must. This can be arranged through observation of charged-current channels with either μ^- or μ^+ in the final state, for instance, through the use of a magnetic field. However, in low-counting experiments such as these, it is also useful to ask whether any information can be gained from putting the neutrino and antineutrino samples together, thus increasing statistics. We define

$$S_N(x) = \frac{U+\overline{U}}{D+\overline{D}}(x). \qquad (27)$$

Note that this does not need charge identification. We show the dependence of S_N on the parameters δ_{32} (both magnitude and sign) and θ_{13} in Fig. 6. We see that the amplitude of oscillation depends weakly on θ_{13} and that it dies down faster for the direct hierarchy than for the inverted hierarchy. It may therefore be possible to determine the mass hierarchy with the sum of neutrino and antineutrino data, but for some-what larger values of the (13) mixing angle, $\theta_{13} \geq 7^\circ$.

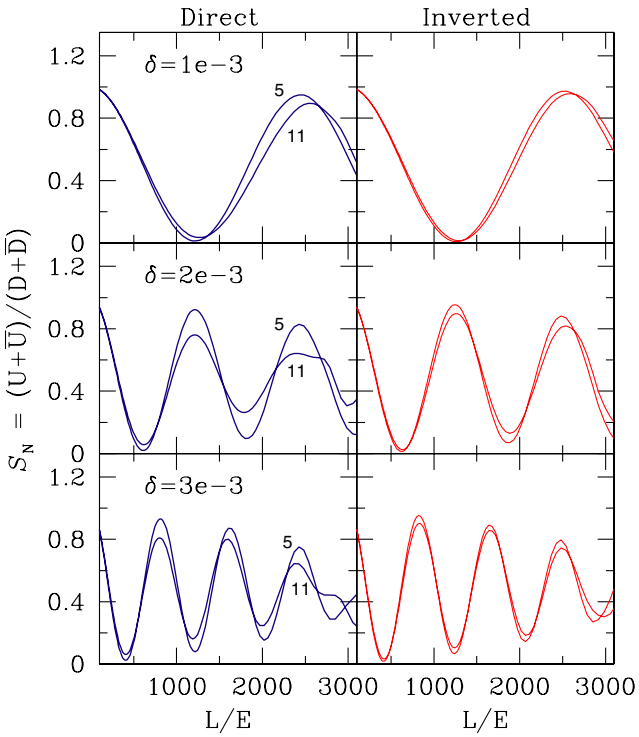

FIG. 6 (color online). The total up/down ratio including both muon-neutrinos and antineutrinos as a function of L/E for $E > 4$ GeV. The three panels correspond to $\delta \equiv |\delta_{32}| = 1, 2, 3 \times 10^{-3}$ eV^2. The best-fit values of other parameters are given in the text. The thick (blue) curves correspond to the direct ($\delta_{32} > 0$) and the thin (red) curves correspond to the inverted ($\delta_{32} < 0$) hierarchy. The curves correspond to $\theta_{13} = 5^\circ$ and 11° as indicated. Curves for in-between values of θ_{13} will lie in-between. Matter effects are more pronounced in the direct hierarchy.

To sum up, the analysis of the up/down events ratio, their difference and their sum, clearly indicates that

(1) the location of the first dip (for neutrinos and antineutrinos with either hierarchy) depends only on the *magnitude* of δ_{32}.
(2) the $\nu_\mu - \overline{\nu}_\mu$ difference asymmetry is almost exactly out of phase for direct and inverted hierarchies in L/E bins whose widths can be optimally determined by a *matter independent* condition involving $|\delta_{32}|$ and L/E.
(3) the *amplitude* of the asymmetry defined above is clearly a sensitive function of θ_{13}.

In the next section we examine the event rates and asymmetries in a realistic magnetised iron calorimeter detector capable of charge identification such as in the MONOLITH, MINOS and ICAL/INO proposals.

IV. EVENT RATES WITH A NEUTRINO GENERATOR

So far we have discussed the theoretical up/down events ratios, a difference asymmetry and its matter sensitivity. We now need to address the question of statistics, i.e., estimate the detector dimension and the time required for data accumulation. We generate events using the NUANCE neutrino generator [13] with the ICAL/INO geometry which consists of 140 layers of 6 cm thick iron plates of transverse section 16 m $\times$ 32 m. The RPCs are sandwiched between the layers. The fiducial mass of the detector is a little under 30 ktons. Results shown correspond to 480 kton-years data and indicate (1) the statistical significance of the events sample (the error bars) and (2) the impact of fluctuations (deviation of the central values from the predictions of the previous section).

The E and L of those neutrinos that undergo charged-current interaction in the detector to produce muons in the final state were directly used to generate the sums and asymmetries. The effect of finite L/E resolution is discussed in the next section. A detailed study reconstructing the neutrino energy and direction from the final state muons and hadrons is in progress.

As stated earlier, it was found that a cut of $E_{\rm min} = 4$ GeV maximizes the relative matter-dependent effect between neutrinos and antineutrinos. While such effects are washed out beyond $E \sim 10$ GeV, we integrated over all possible energies in a bin to improve statistics. Data samples were generated for different values of θ_{13} and δ_{32} (both signs), keeping the other parameters fixed to the values listed in the previous section.

A. The asymmetry

To maximize the asymmetry, it is necessary to integrate the events in a bin size that includes one half-period of the oscillation, where the asymmetry is always positive or negative (see Fig. 5). Unfortunately, this is not easy since different path lengths correspond to different matter densities and the wave-length is density dependent. However, recall that the oscillation wave-length was roughly constant and matter-independent for (anti-)neutrinos with (direct) inverted hierarchy. We therefore identify the bins spanning those L/E corresponding to

$$\frac{1.267|\delta_{32}|L}{E} = n\frac{\pi}{4}; \quad n \text{ odd.} \tag{28}$$

This has the advantage of being matter-independent. Once $|\delta_{32}|$ is measured from the (matter/hierarchy-independent) first minimum in the plot of the U/D ratio as a function of L/E, this can be used to generate the bin sizes for studying the matter-dependent asymmetry.

We exhibit the results for $|\delta_{32}| = 1, 2, 3 \times 10^{-3}$ eV^2 in Figs. 7–9, respectively. In each figure the events asymmetry $\mathcal{A}_N$ is plotted as a function of L/E. In all cases, a zenith angle cut of $|\cos\theta| > 0.1$ was used to remove "horizontal" events, as discussed earlier. The first data point corresponds to a region where no matter effect is expected, that is, up to an L/E smaller than the $n = 1$ value in Eq. (28) above.

The "data" points shown correspond to binning the actual events generated using the NUANCE Monte Carlo

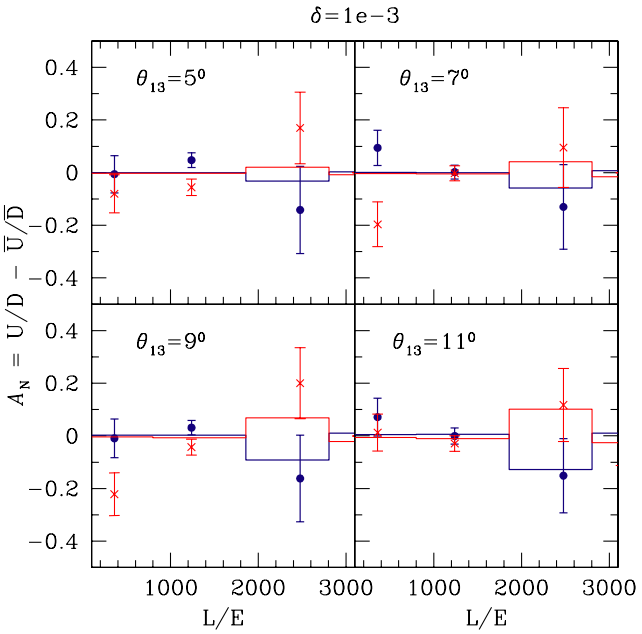

FIG. 7 (color online). The up/down Monte Carlo events asymmetry $\mathcal{A}_N$ integrated over L/E bins shown as a function of L/E. The dots and crosses correspond to the direct and inverted hierarchies, respectively. Error bars shown are obtained from the number of events in each bin. The histograms correspond to the same asymmetry calculated from theory; see Fig. 5. Thick (blue) lines refer to the direct hierarchy and thin (red) ones to the inverted one. The effect of fluctuations is indicated by the shift in the central data values from the histogram. Results are shown for $\theta_{13} = 5, 7, 9, 11$ degrees for $|\delta_{32}| = 1 \times 10^{-3}$ eV2. For more details on the bins, see the text.

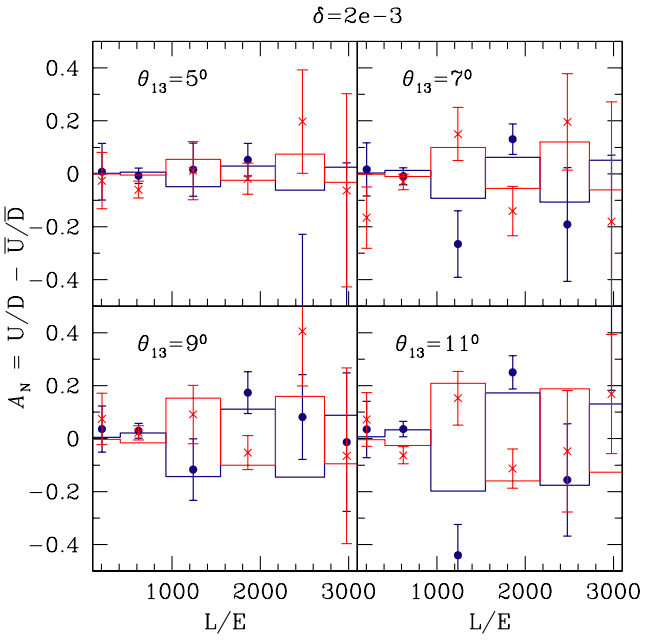

FIG. 8 (color online). The same as Fig. 7 for $|\delta_{32}| = 2 \times 10^{-3}$ eV^2.

event generator in bins whose widths follow the expression Eq. (28). The "dots" and the "crosses" correspond to the direct and inverted hierarchy. The theoretical asymmetry generated by integrating the differential event rate over the bin-width is plotted for comparison as a histogram. The darker lines correspond to the direct hierarchy and lighter ones to the inverted hierarchy. The deviation of the points from the value indicated by the corresponding histogram is an indicator of fluctuations. The size of the error-bar on the data reflects only the statistical error due to the data size in that bin.

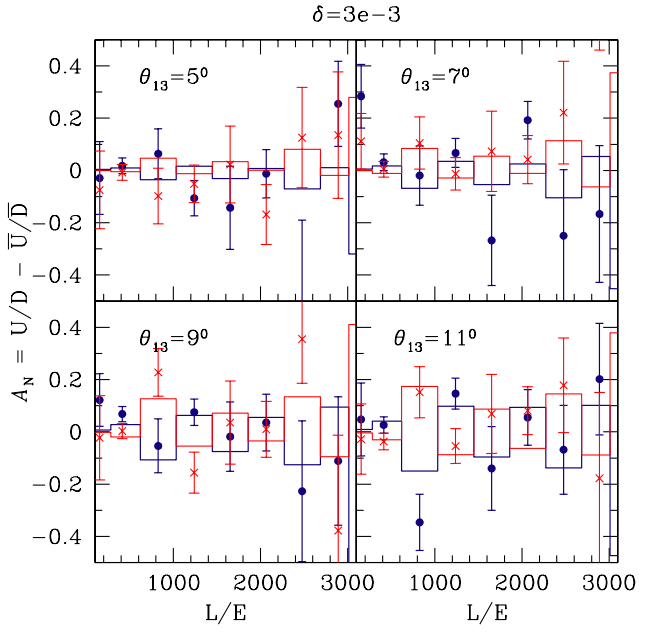

FIG. 9 (color online). The same as Fig. 7 for $|\delta_{32}| = 3 \times 10^{-3}$ eV^2.

The error bars are larger for the inverted than for the direct hierarchy in a given bin. This is because it is the antineutrino event rate that is sensitive to matter effects in the case of inverted hierarchy, as described in Sec. II. Since the antineutrino cross-sections are about a factor of 2 smaller than the neutrino cross-section, the event rates are smaller and the error bars correspondingly larger. Statistically speaking, therefore, it is easier to detect direct than inverted hierarchy.

Results are separately shown for $\theta_{13} = 5, 7, 9, 11$ degrees. It is easily seen that the greatest sensitivity to matter effects occurs for a value of $|\delta_{32}| = 2 \times 10^{-3}$ eV^2. For a smaller $|\delta_{32}|$, the matter effect does not develop significantly until a fairly large L/E, where the event rates begin to drop; for larger $|\delta_{32}|$, the larger number of bins where the asymmetry changes sign leads to smaller statistics per bin.

Note that the first oscillation period (second data point) corresponds to a minimum in the up-coming events rate. In all cases, the largest sensitivity to the hierarchy is therefore in the region around the first maximum in the up/down ratio, or the third bin. In fact, the survival probability is sensitive to matter effects for energies roughly in the range $2 \leq E \leq 10$ GeV. The cut of 4 GeV on the neutrino energy is used to accentuate the asymmetry in the third bin.

A negative (positive) value of asymmetry in this bin clearly indicates direct (inverted) mass hierarchy. It may be possible to improve this result by binning over regions of L/E taking into account modifications due to matter of Eq. (28); in fact, with real data, it may be also be possible to have variable bin sizes, determined by maximizing the magnitude of the asymmetry in each bin. We shall not attempt this here. We only wish to note that the third bin is automatically identified once the magnitude of δ_{32} is determined. It may also be possible to combine the results of several bins (with appropriate sign) to improve the statistics.

Note that with an energy cut $E > 4$ GeV, the events are roughly distributed in the proportion 2.5:2:1 from deep inelastic scattering (DIS), resonance (dominated by 1-pion processes) (RS), and quasielastic (QE) charged-current processes, respectively. There are roughly 3000 events in 480 kton-years, of which about 35% are up-going ones.

Finally, if a nonzero asymmetry is measured, this will yield both the mass hierarchy as well as a lower bound on θ_{13} of at least $\theta_{13} > 6°$ ($\sin^2 2\theta_{13} > 0.04$). While the amplitude of the asymmetry is proportional to $\sin\theta_{13}$, limitations due to statistics make it unlikely that the value of θ_{13} itself will be determined with any reasonable accuracy. One needs to address this issue elsewhere.

B. Asymmetries with finite detector resolution

Inclusion of finite detector resolution reduces the sensitivity, especially beyond the first oscillation minimum and maximum. A straightforward way to include such effects is to smear the observed L and E and observe the impact of this. To this end, we define Gaussian resolution functions for both L and E:

$$R_1(E', E) \equiv \frac{1}{\sqrt{2\pi}\sigma_1} \exp\left[\frac{-(E - E')^2}{2\sigma_1^2}\right];$$
$$R_2(L', L) \equiv \frac{1}{\sqrt{2\pi}\sigma_2} \exp\left[\frac{-(L - L')^2}{2\sigma_2^2}\right]. \quad (29)$$

Hence, the event rate now includes the probability that a neutrino of any possible L' and E' is detected in the detector with path-length L and energy E. We have

$$N_{\rm bin}^{\alpha,R}(x) = \int_{\rm bin} {\rm d}x \int_{E_{\rm min}} \frac{{\rm d}E}{E} \int {\rm d}E' R_1(E', E) \times \int {\rm d}L' R_2(L', L) \frac{{\rm d}^2 N^\alpha}{{\rm d}\ln E' {\rm d}x'}, \quad (30)$$

where[5] $x' = L'/E'$.

We reevaluate the event rates and the up/down asymmetries using this equation, with $\sigma_1 = 0.15E'$ and $\sigma_2 = 0.15L'$. These are realistic widths obtained by a GEANT analysis of atmospheric neutrino events by both the MONOLITH and the ICAL/INO collaborations; this gives a typical FWHM for their ratio (L/E) to be about $\sim 0.4L/E$.

The up/down events ratio (for the case of the direct hierarchy) is shown on the right side of Fig. 10 as a function of L/E for $\delta_{32} = 2 \times 10^{-3}$ eV^2. The results without including resolution functions is shown in the left-hand panel, for comparison. As before, a cut on the neutrino energy of $E > 4$ GeV is applied. With the inclusion of the resolution functions, it is seen that the *amplitude* of the oscillation is greatly damped. Furthermore, the neutrino rates ratio (shown as thick blue lines) is damped much more than that for the antineutrinos (the converse will be true for the inverted hierarchy). Curves correspond to $\theta_{13} = 5, 11°$. Clear oscillations are visible only around the first minimum and maximum.

The resulting asymmetry, that is, the difference of the neutrino and antineutrino events ratios, $\mathcal{A}_N$, is plotted in Fig. 11. Again, the panels on the right correspond to the rates calculation including resolution, while those on the left correspond to rates without including resolution effects. There is virtually no difference for small L/E. In general, however, the amplitude of the asymmetry decreases although it is still largest in the second envelope (corresponding to the third bin in the earlier discussions).

[5]The combination of Gaussian resolution functions for L and E integrates to a Lorentzian in their ratio provided the integration over *all* variables is unrestricted. We need to specify individual resolution functions here because of the cut on E.

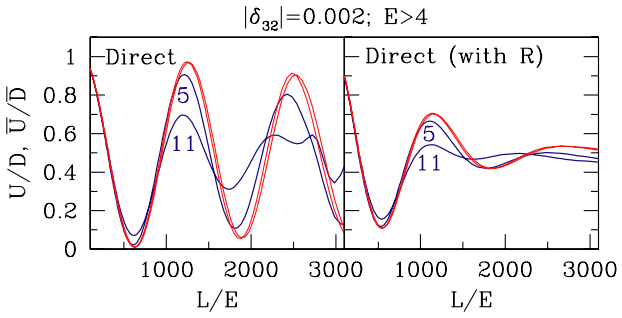

FIG. 10 (color online). A comparison of the up/down events ratio as a function of L/E (for the direct hierarchy) with (right) and without (left) the inclusion of Gaussian resolution functions for $|\delta_{32}| = 2 \times 10^{-3}$ eV^2 and $\theta_{13} = 5, 11°$. Results are very sensitive to the widths of the Gaussian used. The results presented correspond to a Gaussian width $\sigma = 15\%$ for both L and E. The thick (blue) curves correspond to neutrinos and the thin (red) curves to the antineutrinos; note that the latter are barely discernible from each other.

It is seen that the asymmetry is larger with a cut of $E_{\rm min} = 4$ GeV than with a cut of $E_{\rm min} = 2$ GeV while the *number of events* is smaller by roughly half in the case of the larger energy cut. In particular, by lowering the cut to $E_{\rm min} = 2$ GeV, not only does the sample size effectively double, the contribution from various processes changes to the proportion 1:1.5:1 from 2.5:2:1 for DIS, RS and QE processes.

Thus there are two conflicting requirements: to enhance the size of the asymmetry, we need a larger value of $E_{\rm min}$, but to improve statistics, we need a larger sample size. The final choice of $E_{\rm min}$ should optimize these two requirements.

We note in passing that, for $E_{\rm min} = 4$ GeV, there is a fairly large asymmetry for large L/E as well; the statistical significance in this bin is however small. In both cases, the asymmetry in the penultimate envelope is almost vanishingly small; the oscillation length in this case is also very small.

In short, it appears that a finite resolution function causes smearing of the data across bins in such a way that the magnitude of the asymmetry becomes significantly smaller, and even vanishes beyond the third envelope/bin. We can improve the result by summing the asymmetries over several envelopes. We define

$$\mathcal{A}_n^H = \sum_{i=1}^{n} (-1)^i \mathcal{A}_N^{H,i}, \quad (31)$$

where H corresponds to a given hierarchy, direct, or inverted, $H = D, I$. Typically, $\mathcal{A}_N^D \sim -\mathcal{A}_N^I$ in a bin, and therefore the sum in Eq. (31) is roughly equal and opposite for the two hierarchies. Furthermore, the statistics are not very different with either hierarchy. The significance of the result is thus estimated by comparing the difference

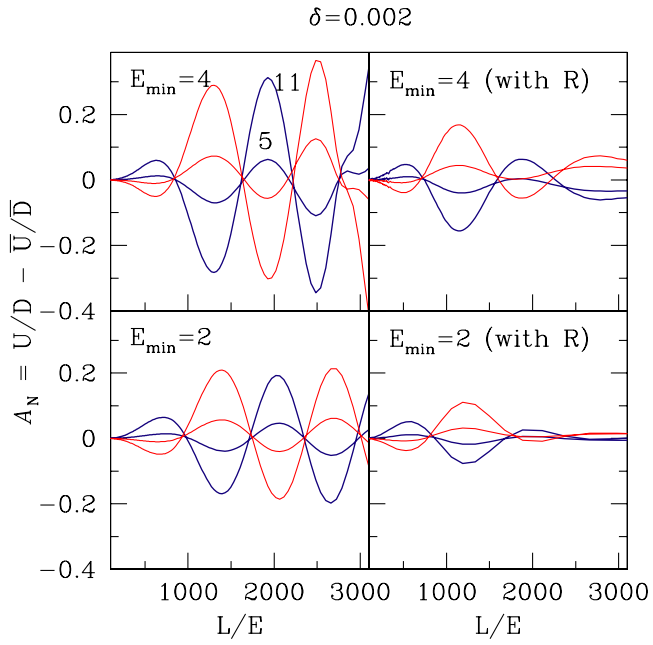

FIG. 11 (color online). A comparison of the difference asymmetry as in Fig. 5 with (right) and without (left) inclusion of resolution functions for $\delta \equiv |\delta_{32}| = 2 \times 10^{-3}$ eV^2 and $\theta_{13} = 5, 11°$. The thick (blue) curves correspond to the direct and the thin (red) curves to the inverted hierarchy. Two cases, $E > 4$ and $E > 2$ GeV, are shown. It is clear that the higher energy cut better emphasises the asymmetry and hence the matter effects; however, the event rates are roughly halved in this case, for the same exposure times.

$$\Delta\mathcal{A}_n = \mathcal{A}_n^D - \mathcal{A}_n^I \tag{32}$$

with the error σ corresponding to a given exposure. In fact, the ratio $\Delta\mathcal{A}_n/\sigma$ indicates the probability of the observed asymmetry being assigned to the correct hierarchy.

The error σ arises primarily from statistics. This is because the asymmetry is defined as a difference of two ratios. Systematic errors (due to uncertainties both in fluxes and cross-sections) in the ratio are therefore very small and can be ignored; this was pointed out very early on by the MONOLITH collaboration [10].

We list the values of $\Delta\mathcal{A}_n$ and the corresponding statistical error σ_n (we have chosen the larger of the errors for the direct and inverted hierarchy) in Tables I, II, and III, for different resolutions in E and L of 15%, 10%, and 5%, respectively. In each table, results for both $n = 2$ and $n = 3$ (that is, a sum over two or three envelopes), corresponding to $|\delta_{32}| = 2.0 \times 10^{-3}$ eV^2 and $\theta_{13} = 7, 9, 11, 13°$ are shown for different exposures of 480, 800 and 1120 kton-years, respectively. The resulting confidence level of the measurement is also indicated in the tables.

It is clear that the asymmetry and hence $\Delta\mathcal{A}_n$ increases with θ_{13}, *independent* of exposure. The effect of increasing the exposure is to improve the errors, without changing the central values of the asymmetry. This can be seen by comparing results for the same θ_{13} in each table. Since the minimum exposure of 480 kton-years is already large, and statistical errors improve only as $\sqrt{N_{data}}$, it will be difficult to greatly enhance the significance of the result by going to larger and larger exposures.

The effect of improving the resolution function (obtained by comparing the same row in the Tables I, II, and III), is two-fold. For a given exposure, improving the resolution function (by which we mean improving the Gaussian widths of the resolutions in E and L as defined in Eq. (29) above) *increases the central value of the asymmetry* in each case. It also results in marginally improved errors for $n = 3$, that is, when summing over all the three significant bins in the L/E distribution, which further

TABLE I. Significance of the asymmetry for different exposures in kton-years for resolution widths $\sigma_{1,2}$ in E and L (see Eq. (29)) of 15%. Asymmetries are shown for typical values of $\theta_{13} = 7, 9, 11, 13°$; the CHOOZ bound limits this angle to $\theta_{13} \leq 14.9°$.

Exposure (kton-years)	$\Delta\mathcal{A}_2$ (CL%)	$\Delta\mathcal{A}_3$ (CL%)
$\theta_{13} = 7°$		
480	$0.166 \pm 0.161(1.0\sigma, 68.3\%)$	$0.167 \pm 0.230(0.7\sigma, 51.6\%)$
800	$0.166 \pm 0.125(1.3\sigma, 80.6\%)$	$0.167 \pm 0.178(0.9\sigma, 63.2\%)$
1120	$0.166 \pm 0.105(1.6\sigma, 89.0\%)$	$0.167 \pm 0.151(1.1\sigma, 72.9\%)$
$\theta_{13} = 9°$		
480	$0.257 \pm 0.159(1.6\sigma, 89.0\%)$	$0.280 \pm 0.230(1.2\sigma, 77.0\%)$
800	$0.257 \pm 0.123(2.1\sigma, 96.4\%)$	$0.280 \pm 0.178(1.6\sigma, 89.0\%)$
1120	$0.257 \pm 0.104(2.5\sigma, 98.8\%)$	$0.280 \pm 0.150(1.9\sigma, 94.3\%)$
$\theta_{13} = 11°$		
480	$0.357 \pm 0.157(2.3\sigma, 97.9\%)$	$0.415 \pm 0.230(1.8\sigma, 92.8\%)$
800	$0.357 \pm 0.122(2.9\sigma, 99.6\%)$	$0.415 \pm 0.178(2.3\sigma, 97.9\%)$
1120	$0.357 \pm 0.103(3.5\sigma, 99.95\%)$	$0.415 \pm 0.150(2.8\sigma, 99.6\%)$
$\theta_{13} = 13°$		
480	$0.459 \pm 0.155(3.0\sigma, 99.7\%)$	$0.560 \pm 0.230(2.4\sigma, 99.4\%)$
800	$0.459 \pm 0.120(3.8\sigma, 99.98\%)$	$0.560 \pm 0.178(3.1\sigma, 99.8\%)$
1120	$0.459 \pm 0.102(4.5\sigma, 99.999\%)$	$0.560 \pm 0.151(3.7\sigma, 99.98\%)$

TABLE II. Same as Table I for resolution widths $\sigma_{1,2}$ in E and L (see Eq. (29)) of 10%.

Exposure (kton-years)	$\Delta\mathcal{A}_2$ (CL%)	$\Delta\mathcal{A}_3$ (CL%)
$\theta_{13} = 7°$		
480	$0.185 \pm 0.167(1.1\sigma, 72.9\%)$	$0.232 \pm 0.220(1.1\sigma, 72.9\%)$
800	$0.185 \pm 0.130(1.4\sigma, 83.8\%)$	$0.232 \pm 0.170(1.4\sigma, 83.8\%)$
1120	$0.185 \pm 0.110(1.7\sigma, 91.1\%)$	$0.232 \pm 0.144(1.6\sigma, 89.0\%)$
$\theta_{13} = 9°$		
480	$0.287 \pm 0.165(1.7\sigma, 91.1\%)$	$0.384 \pm 0.220(1.8\sigma, 92.8\%)$
800	$0.287 \pm 0.128(2.2\sigma, 97.2\%)$	$0.384 \pm 0.170(2.3\sigma, 97.9\%)$
1120	$0.287 \pm 0.108(2.7\sigma, 99.3\%)$	$0.384 \pm 0.144(2.7\sigma, 99.3\%)$
$\theta_{13} = 11°$		
480	$0.399 \pm 0.163(2.4\sigma, 98.4\%)$	$0.565 \pm 0.221(2.6\sigma, 99.1\%)$
800	$0.399 \pm 0.126(3.2\sigma, 99.9\%)$	$0.565 \pm 0.171(3.3\sigma, 99.9\%)$
1120	$0.399 \pm 0.107(3.7\sigma, 99.98\%)$	$0.565 \pm 0.144(3.9\sigma, 99.99\%)$
$\theta_{13} = 13°$		
480	$0.515 \pm 0.161(3.2\sigma, 99.9\%)$	$0.758 \pm 0.223(3.4\sigma, 99.9\%)$
800	$0.515 \pm 0.125(4.1\sigma, 99.996\%)$	$0.758 \pm 0.173(4.4\sigma, 99.999\%)$
1120	$0.515 \pm 0.102(4.9\sigma, 99.9999\%)$	$0.758 \pm 0.146(5.2\sigma, 100\%)$

TABLE III. Same as Table I for resolution widths $\sigma_{1,2}$ in E and L (see Eq. (29)) of 5%.

Exposure (kton-years)	$\Delta\mathcal{A}_2$ (CL%)	$\Delta\mathcal{A}_3$ (CL%)
$\theta_{13} = 7°$		
480	$0.198 \pm 0.172(1.1\sigma, 72.9\%)$	$0.297 \pm 0.209(1.4\sigma, 83.8\%)$
800	$0.198 \pm 0.133(1.5\sigma, 86.6\%)$	$0.297 \pm 0.162(1.8\sigma, 92.8\%)$
1120	$0.198 \pm 0.112(1.8\sigma, 92.8\%)$	$0.297 \pm 0.137(2.2\sigma, 97.2\%)$
$\theta_{13} = 9°$		
480	$0.308 \pm 0.170(1.8\sigma, 92.8\%)$	$0.489 \pm 0.209(2.3\sigma, 97.9\%)$
800	$0.308 \pm 0.132(2.3\sigma, 97.9\%)$	$0.489 \pm 0.162(3.0\sigma, 99.7\%)$
1120	$0.308 \pm 0.111(2.8\sigma, 99.6\%)$	$0.489 \pm 0.137(3.6\sigma, 99.97\%)$
$\theta_{13} = 11°$		
480	$0.429 \pm 0.168(2.5\sigma, 98.8\%)$	$0.717 \pm 0.213(3.4\sigma, 99.9\%)$
800	$0.429 \pm 0.130(3.3\sigma, 99.9\%)$	$0.717 \pm 0.165(4.3\sigma, 99.9983\%)$
1120	$0.429 \pm 0.110(3.9\sigma, 99.99\%)$	$0.717 \pm 0.139(5.1\sigma, 100\%)$
$\theta_{13} = 13°$		
480	$0.554 \pm 0.166(3.3\sigma, 99.9\%)$	$0.960 \pm 0.218(4.4\sigma, 99.999\%)$
800	$0.554 \pm 0.128(4.3\sigma, 99.998\%)$	$0.960 \pm 0.169(5.7\sigma, 100\%)$
1120	$0.554 \pm 0.109(5.1\sigma, 100\%)$	$0.960 \pm 0.143(6.7\sigma, 100\%)$

enhances the significance of the result. For example, the improvement upon increasing the exposure from 480 to 1120 kton-years at 15% resolution is similar to that obtained by improving the resolution, *at 480 kton-years*, from 15% to 10%.

Note also that the significance of the results for $\Delta\mathcal{A}_2$ is higher than for $\Delta\mathcal{A}_3$ for larger resolutions of 15%; this may imply that best results are obtained from single-bin information when the resolutions are poorer. Also, it turns out that the results are systematically better for a cut of $E_{min} = 4$ GeV rather than for a cut of 2 GeV.

While resolutions with widths of 10% may not be hard to achieve, it is not clear whether it is possible to reach 5%. One way is to exclude the DIS events (perhaps by cutting out events with large hadronic activity). The resulting data set is smaller by about 45%; however, it may be possible to resolve the energy and direction of the neutrino much better since there are only quasielastic and resonance events left in the sample. This needs to be studied in more detail.

In summary, it appears that, even for moderate to large exposures, it may be difficult to achieve effects larger than 2σ or so, unless of course Nature is kind and prefers large θ_{13}. For $\theta_{13} \geq 9°$, a significance of 99.3% (nearly 3σ) or more is obtained with an exposure of 800 (1120) kton-years and resolutions in both energy and angle of 5% (10%). It is clear that a prior knowledge of θ_{13} from some other experiment would greatly facilitate the extraction of the mass hierarchy since the magnitude of the expected asymmetry would then be known.

In short, the major features of the analysis without including finite detector resolutions appear to hold,

although with much reduced significance. A *prima facie* case has been made for determining mass hierarchy through observation of atmospheric neutrinos with ICAL detectors; however, the effect is small and is difficult to measure. Indeed, it is clear that the asymmetry is very sensitive to smearing in both L and E. Our study indicates that an *improvement in the detector resolution* has a stronger impact on the results than a mere enhancement in size or the number of years of data-accumulation. A detailed study involving actual reconstruction of muon and hadron energies and muon direction is needed to determine the ultimate sensitivity of such a detector to the issue of hierarchy.

C. The Sum

The results from the sum of neutrino and antineutrino events S_N are much less sensitive to matter effects, as expected. Results (with same cuts as above) are shown in Figs. 12–14 for $|\delta_{32}| = 1, 2, 3 \times 10^{-3}$ eV^2 respectively. For large values of $\theta_{13} > 7°$, the amplitude of the sum averages to 1/2 much faster for the direct hierarchy. The numerical study will need to be carefully done to establish the significance of this result.

V. DISCUSSION

We have discussed the possibility of obtaining information on the mixing angle θ_{13} and the sign of δ_{32} using a magnetized iron calorimeter collecting data on atmospheric muon-neutrinos, capable of charge identification. It appears that such a detector will be sensitive to the neutrino mass hierarchy only if $\theta_{13} > 6°$ $\sin^2 2\theta_{13} > 0.04$).

We have defined a difference asymmetry in Eq. (22) as the difference between the up/down rates of neutrinos and antineutrinos. By taking the up/down ratio, the systematic errors are greatly reduced. In particular, the uncertainty in the overall flux normalization is removed. Such a ratio also minimizes the dependence on the cross-section, which is substantially different for neutrinos and antineutrinos in the GeV energy range of interest. As a consequence, the measurable rate asymmetry is related to a theoretical flux-weighted probability (difference) asymmetry given in Eq. (24). Examination of the theoretical asymmetry immediately suggests ways of binning the data in order to maximize the asymmetry in each bin (in L/E). It turns out that the *sign of the asymmetry* is sensitive to the neutrino mass hierarchy (that is, the sign of $\delta_{32} = m_3^2 - m_2^2$) while its magnitude is sensitive to the (13) mixing angle θ_{13}.

We summarize our conclusions below.

(i) The limits on $|\delta_{32}|$ and $\sin 2\theta_{23}$ may be reliably obtained using the location of the first minimum and the amplitude of first oscillation of a plot of the ratio of up/down events as a function of L/E. While no detailed discussion on this issue has been presented here, it has been well-established elsewhere [10,12].

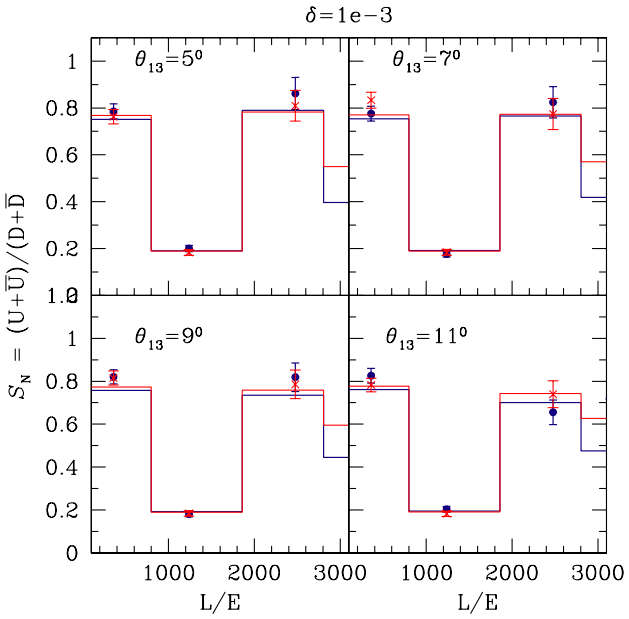

FIG. 12 (color online). The up/down ratio S_N of the sum of neutrino and antineutrino events integrated over L/E bins shown with statistical errors as a function of L/E. Results are shown for $\theta_{13} = 5, 7, 9, 11$ degrees for $|\delta_{32}| = 1 \times 10^{-3}$ eV^2. For more details, see the caption of Fig. 7.

The detector mass-exposure required for this purpose is about 150 kton-years. While charge identification is not crucial for this step, presence of a magnetic field helps in obtaining better energy resolution. This step however is *not dependent* on the value of θ_{13} or the sign of δ_{32}.

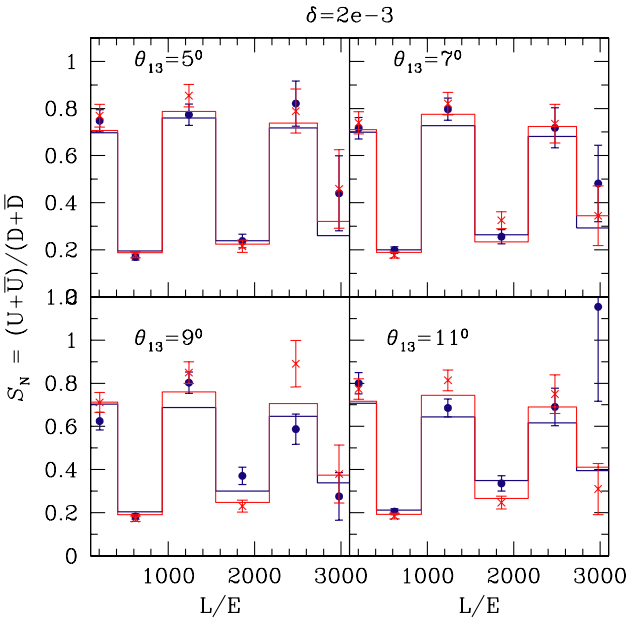

FIG. 13 (color online). The same as Fig. 12 for $|\delta_{32}| = 2 \times 10^{-3}$ eV^2.

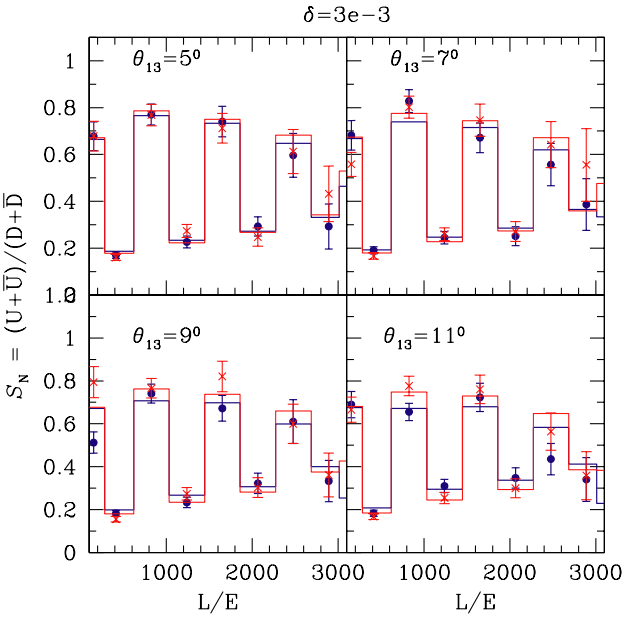

FIG. 14 (color online). The same as Fig. 12 for $|\delta_{32}| = 3 \times 10^{-3}$ eV^2.

(ii) If θ_{13} is larger than 6°, then the pattern of subsequent oscillations after the first dip can give definite indication about the hierarchy through the difference asymmetry as discussed above. It is possible to maximize the sensitivity to this asymmetry in fixed L/E bins (improve statistical significance) by applying an energy cut, $E_{\rm min} > 4$ GeV. An optimum $|\delta_{32}|$ dependent bin-width can be determined that is *matter-independent*. This is easily accomplished as $|\delta_{32}|$ can be well determined independently as discussed above.
For direct hierarchy the matter effects dominate through the neutrinos which have a higher cross-section and hence give more pronounced matter effects. If the matter effects are small even when θ_{13} is large, then it is a clear indication of inverted hierarchy since the dominant neutrino events will have less impact due to matter.

(iii) Inclusion of finite detector resolution reduces the sensitivity, especially beyond the first oscillation minimum and maximum in L/E. A combination of enhanced exposure and improved resolution will still enable a measurement of the mass hierarchy, provided θ_{13} is not too small, $\theta_{13} > 6°$. The best scenario is when θ_{13} is already established from other experiments to be in the favorable range. Of course, in the absence of such a measurement, nonobservation of the asymmetry can put a lower bound on θ_{13} while leaving open the issue of the hierarchy.

(iv) It is therefore important to maximize the sensitivity of the detector to the range of L/E where the matter effects are significant. It may be interesting to consider a nonhorizontal detector geometry in order to maximize the sensitivity to the relevant L/E bins; typically, these correspond to an average path-length L around 7000 km. If neutrinos with such path-lengths are to be transverse to the iron-plates, a geometry with plates tilted at about 33° to the horizontal may be preferred. This needs more careful study.

While many experiments (present and proposed) will be sensitive to the (13) mixing angle θ_{13}, it appears that charge identification may be essential for settling the issue of the mass hierarchy. In this context we note that reactor neutrino experiments are not sensitive to matter effects and will be complementary to an ICAL detector. Short-baseline accelerator experiments may also not be as sensitive to matter effects. Long-baseline experiments with neutrino factory beams can surely settle this issue, and are sensitive to much smaller values of θ_{13}, but are expected to come online at much later times.

Thus a study of atmospheric neutrinos with a magnetised iron calorimeter detector can, in principle, provide fundamental information on the parameters of the neutrino mixing matrix and the neutrino mass-squared differences; in particular, it may resolve the question of hierarchy in the neutrino masses. It is certain that large exposures (more than 500 kton-years) will be required to obtain a result with a significance of at least 90% CL. In addition, good resolution in both energy and angle discrimination is required. For larger $\theta_{13} \geq 9°$, a significance of 99.3% (nearly 3σ) or more is obtained with an exposure of 800 (1120) kton-years and resolutions in both energy and angle of 5% (10%). Results for smaller θ_{13} remain at the (2σ) 95% CL even in the best-case scenario. Hence the practical issue of experimental feasibility seems much harder to resolve.

ACKNOWLEDGMENTS

We are grateful to Dave Casper for making the NUANCE software freely available, and answering a long list of questions on its use. We are grateful to the members of the INO group, and, in particular, to the members of the INO group at IMSc, K. Kar, H. S. Mani, G. Rajasekaran, and Abdul Salam for many discussions and encouragement. We also thank G. Rajasekaran for a careful and critical reading of the manuscript and many suggestions for its improvement. We thank Nita Sinha and Probir Roy for pointing out errors in some analytical formulas of Section IIB.

[1] SNO Collaboration, S. N. Ahmed *et al.*, Phys. Rev. Lett. **92**, 181301 (2004); SNO Collaboration, Q. R. Ahmad *et al.*, Phys. Rev. Lett. **89**, 011302 (2002); Phys. Rev. Lett. **89**, 0113010 (2002); Phys. Rev. Lett. **87**, 071301 (2001); Super-Kamiokande Collaboration, S. Fukuda *et al.*, Phys. Lett. B **539**, 179 (2002); Super-Kamiokande Collaboration, Phys. Rev. Lett. **86**, 5651 (2001); Super-Kamiokande Collaboration, Y. Fukuda *et al.*, Phys. Rev. Lett. **82**, 2430 (1999); Super-Kamiokande Collaboration, Y. Fukuda *et al.*, Phys. Rev. Lett. **82**, 1810 (1999); Y. Fukuda *et al.*Phys. Rev. Lett. **81**, 1158 (1998); GALLEX Collaboration, W. Hampel *et al.*, Phys. Lett. B **447**, 127 (1999); SAGE Collaboration, J. N. Abdurashitov *et al.*, Phys. Rev. Lett. **83**, 4686 (1999); Kamiokande-II Collaboration, K. S. Hirata *et al.*, Phys. Rev. D **44**, 2241 (1991); Homestake, R. Davis, Prog. Part. Nucl. Phys. **32**, 13 (1994).

[2] Super-Kamiokande Collaboration, Y. Fukuda *et al.*, Phys. Rev. Lett. **81**, 1562 (1998).

[3] KamLAND Collaboration, K. Eguchi *et al.*, Phys. Rev. Lett. **90**, 021802 (2003); CHOOZ Collaboration, M. Apollonio *et al.*, Eur. Phys. J. C **27**, 331 (2003).

[4] Super-Kamiokande Collaboration, Y. Ashie *et al.*, Phys. Rev. Lett. **93**, 101801 (2004); Super-Kamiokande Collaboration, M. Ishitsuka, in *The 5th Workshop on "Neutrino Oscillations and their Origin", 2004, Tokyo, Japan* (unpublished).

[5] B. Pontecorvo, Zh. Eksp. Teor. Fiz. **33**, 549 (1957); Sov. Phys. JETP, **6**, 429 (1957).

[6] Z. Maki, M. Nakagawa, and S. Sakata, Prog. Theor. Phys. **28**, 870 (1962).

[7] K2K Collaboration, M. H. Ahn *et al.*, Phys. Rev. Lett. **90**, 041801 (2003).

[8] T. Tabarelli de Fatis, Eur. Phys. J. C **24**, 43 (2002).

[9] Sergio Palomares-Ruiz and S. T. Petcov, hep-ph/0406096.

[10] N. Y. Agafonova *et al.*, http://castore.mib.infn.it/~monolith/proposal/.

[11] A. Para, Acta Phys. Pol. B **31**, 1313 (2000); C. Andreopoulos, P. Stamoulis, and G. Tzanakos, http://www-numi.fnal.gov/.

[12] G. Rajasekaran, hep-ph/0402246.

[13] D. Casper, Nucl. Phys. B, Proc. Suppl. **112**, 161 (2002).

[14] M. Honda, T. Kajita, K. Kasahara, and S. Midorikawa, Phys. Rev. D **64**, 053011 (2001).

[15] J. N. Bahcall, M. C. Gonzalez-Garcia, and C. Peña-Garay, J. High Energy Phys. 02 (2003) 009; M. C. Gonzalez-Garcia, hep-ph/0211054.

[16] M. C. Gonzalez-Garcia and Y. Nir, Rev. Mod. Phys. **75**, 345 (2003).

[17] P. Picchi and F. Pietropaolo, SCAN-9710037.

[18] V. D. Barger, S. Pakvasa, K. Whisnant, and R. J. N. Phillips, Phys. Rev. D **22**, 2718 (1980).

[19] A. M. Dziewonski and D. L. Anderson, Phys. Earth Planet. Inter. **25**, 297 (1981).

[20] P. Huber and W. Winter, Phys. Rev. D **68**, 037301 (2003).